Review Article

Nano Research
2024, 17(12): 10332–10345

ISSN 1998-0124 CN 11-5974/O4
https://doi.org/10.1007/s12274-024-6504-x

Single quantum dot spectroscopy for exciton dynamics

Bin Li[1], Guofeng Zhang[2] (✉), Yuke Gao[1], Xiaopeng chen[1], Ruiyun Chen[2], Chengbing Qin[2], Jianyong Hu[2], Ruixiang Wu[1], Liantuan Xiao[2] (✉), and Suotang Jia[2]

[1] *Key Laboratory of Spectral Measurement and Analysis of Shanxi Province, College of Physics and Information Engineering, Shanxi Normal University, Taiyuan 030031, China*

[2] *State Key Laboratory of Quantum Optics and Quantum Optics Devices, Institute of Laser Spectroscopy, Collaborative Innovation Center of Extreme Optics, Shanxi University, Taiyuan 030006, China*

Received: 29 November 2023 / **Revised:** 10 January 2024 / **Accepted:** 18 January 2024

ABSTRACT

Colloidal semiconductor quantum dots (QDs) exhibit broadband light absorption, continuously tunable narrowband emission, and high photoluminescence quantum yields. As such, they represent promising materials for use in light-emitting diodes, solar cells, detectors, and lasers. Single-QD spectroscopy can remove the ensemble averaging to reveal the diverse optical properties and exciton dynamics of QD materials at the single-particle level. The results of relevant research can serve as guidelines for materials science community in tailoring the synthesis of QDs to develop novel applications. This paper reviews recent progress in exciton dynamics revealed by single-QD spectroscopy, focusing on the exciton and multi-exciton dynamics of single colloidal CdSe-based QDs and perovskite QDs. Finally, potential future directions for single-QD spectroscopy and exciton dynamics are briefly considered.

KEYWORDS

single quantum dot spectroscopy, exciton dynamics, single exciton, photoluminescence blinking, biexciton

1 Introduction

Colloidal semiconductor quantum dots (QDs) typically consist of inorganic cores and organic ligand molecules. Their sizes are either smaller than or in close proximity to the Bohr radius of excitons, and their nanostructures can bind excitons in three spatial dimensions. Thanks to the quantum confinement effect of QDs, they possess a discrete energy level structure similar to atomic properties. Colloidal semiconductor QDs possess advantages, including broadband absorption, narrow emission bandwidth, high photoluminescence (PL) quantum yield, adjustable emission wavelength, and convenient solution processing [1, 2]. QDs can be used as high-quality materials for the preparation of optoelectronic devices such as light-emitting diodes, solar cells, detectors, lasers, and quantum light sources [3–7]. The PL properties of colloidal semiconductor QDs are greatly affected by their size, morphology, core–shell structure, surface ligands, and local environment. Even QDs produced in the same batch exhibit significant differences. It is important to take all these factors into account when preparing QDs for optimal application in optoelectronic devices. Achieving precise measurement of these variations is a fundamental issue in research across materials science, crystallography, and interface chemistry. Accurate measurement and characterization of the photophysical properties of QDs are essential for preparing high-quality QDs with uniform scale and achieving their intended applications. While transmission electron microscopy is capable of effectively characterizing the morphology of QDs, it is unable to provide information regarding their optical properties [8–10]. Traditional time-resolved PL spectroscopy allows measurement of certain differences in QDs, such as spectral broadening in ensemble samples and PL decay curves showing multi-exponential forms [11, 12]. However, these properties are determined by measuring the QD ensemble system, and the results acquired represent an average of the optical characteristics of all QDs within the measurement area. The fast-evolving technology of single-QD spectroscopy enables the measurement of PL dynamics in one QD, thus providing accurate material differentiation data. Analysis of the PL properties of single QDs provides insight into the influence of various components, particle size, morphology, core–shell structure, surface defects, surface ligands, and local environment of QDs on their PL characteristics [13–16]. Consequently, the obtained results from single QD-spectroscopy have the potential to effectively guide the design of QD materials and contribute to the preparation of high quality QD materials with uniform size and excellent luminescence properties.

A single exciton can be formed in a QD when an electron from the valence band (VB) is excited into the conduction band (CB), leaving a hole where the electron and hole are attracted by the Coulomb force [17, 18]. When two or more excitons are present simultaneously in a single QD, a biexciton or multi-exciton state is formed [19]. The dimensions of QDs are typically only a few nanometers, which significantly enhances the carrier–carrier Coulomb interactions. Therefore, multi-excitons in QDs mainly recombine in the form of an Auger process, i.e., the electron-hole recombination energy is not emitted as a photon, but is transferred to a third carrier. Therefore, the quantum yield of multi-excitons is typically much lower than that of single exciton

Address correspondence to Guofeng Zhang, guofeng.zhang@sxu.edu.cn; Liantuan Xiao, xlt@sxu.edu.cn

[20, 21]. Besides, multi-excitons often have extremely lower formation probability in comparison to single excitons [22]. Therefore, studying multi-exciton dynamics of single QDs remains a challenging task. The investigation into exciton and multi-exciton dynamics of single QDs is highly important, as it contributes to the advancement of applications using colloidal QDs [23].

This paper reviews the recent progress in the exciton dynamics revealed by single-QD spectroscopy and discusses several new methods for measuring and manipulating exciton dynamics at the single-QD level. The topics covered include the PL blinking dynamics and control of blinking, exciton and multiexciton dynamics, and manipulation of biexciton emission. Finally, the potential future direction of single QD-spectroscopy and exciton dynamics is briefly addressed.

2 Basic equipment and methods for single-QD sectroscopy

Advances in optical microscopy have enabled routine observation of the PL of a single QD using highly sensitive photodetectors. Confocal microscopy is typically used for single-QD measurements, as shown in Fig. 1. The experimental optical path involves the laser passing through an excitation filter, a 1/2 wave plate, and a 1/4 wave plate, before being reflected by a dichroic mirror and focused onto the QD sample by an objective lens. The PL of the QD sample is collected through the objective lens and passes through a dichroic mirror, an emission filter, and a pinhole, and is finally split by a beam splitter and detected by two single-photon counting modules (SPCMs) [13, 21, 24]. To ensure accurate measurements, it is crucial to select appropriate excitation filter, dichroic mirror, and emission filter based on the absorption and emission wavelengths of the QD samples. The excitation filter serves to eliminate stray light from the laser. The dichroic mirror separates the laser from the PL of the QDs. It reflects the short-wavelength laser and transmits the long-wavelength PL. The emission filter is then used to filter out the PL of the QDs. To achieve single QD detection, the optical path must be adjusted so that the position of the pinhole and the focus of the objective lens are confocal. The benefit of this is that it can eliminate out-of-focus photons and enhance the signal-to-noise ratio. The beam splitter's role is to divide the PL into two detectors with equal probability for Hanbury Brown–Twiss (HBT) detection.

Time-tagged, time-resolved, and time-correlated single-photon counting (TTTR-TCSPC) technology is a powerful tool in the single-QD spectroscopy. This technology allows for the accurate recording of the arrival time of each photon detected by the SPCMs during single QD measurement, with precision up to the picosecond level. Post-processing the data obtained from TTTR-TCSPC technology can provide important experimental data of a single QD: PL intensity trace and PL decay curve. The PL intensity trace is obtained by monitoring the change in the number of detected PL photons per second. The PL decay trace is a histogram constructed from the arrival time of every detected photon. By combining PL intensity trace and the PL decay curve, the exciton recombination dynamics of single QDs can be effectively studied.

3 Single exciton recombination dynamics of single QDs

The PL intensity trajectory of a single QD primarily arises from the single exciton emission due to the strong nonradiation Auger recombination and the low formation probability of multi-excitons. Analysis of the PL intensity trajectories can provide valuable information about the single exciton, such as its quantum yield, exciton lifetime, as well as evolution with time. In weak light excitation conditions, the PL of QDs mainly results from the radiative recombination of single excitons. The quantum yield of single exciton is proportional to the PL intensity. Therefore, the changing trend of the quantum yield can be observed from the PL trajectory. Also under weak light excitation conditions, the lifetime of single exciton can be determined by fitting the PL decay trace. In addition, by studying the correlation between the PL intensity and lifetime of single excitons over time, the PL blinking mechanisms of single QDs can be revealed.

3.1 PL blinking dynamics of single QDs

Under constant illumination, a single QD's PL intensity fluctuates between bright (on) and dark (off) states, a phenomenon known as PL blinking [25, 26]. PL blinking is a phenomenon unique to single particles (e.g., single molecules, single QDs, single perovskite crystals, and single nanoplatelets) [27–31]. Studying PL blinking is essential to comprehend the recombination dynamics of single exciton in QDs [32]. The origin of PL blinking can be effectively revealed through the correlation between the PL intensity and lifetime of single QDs. Recent advances have classified PL blinking mechanisms of QDs into three main types: Auger-blinking, band-edge carrier (BC) blinking, and hot-carrier (HC) blinking.

The Auger-blinking of single QDs can be described by the charging and discharging model of QDs [33, 34]. Under photoexcitation, QD has a likelihood undergoing photoionization, that is, the electron (or hole) in the excitons is ionized. The remaining hole (or electron) combines with the newly generated electron-hole pair, forming a positive (or negative) trion state, a three-particle state, as shown in Fig. 2(a). The trion states decay mainly by non-radiative Auger recombination, transferring their energy to an extra electron or hole, ultimately leading to a decline in PL intensity and lifetime. When single QD undergoes the ionization and deionization process, PL switching between the

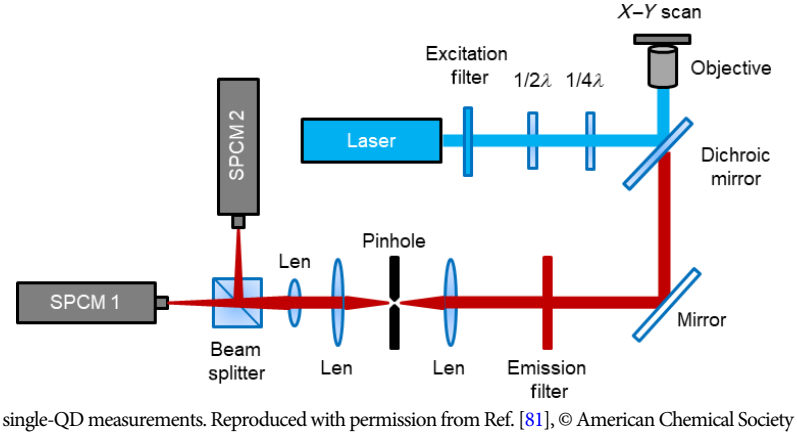

Figure 1 Experimental setup for single-QD measurements. Reproduced with permission from Ref. [81], © American Chemical Society 2020.

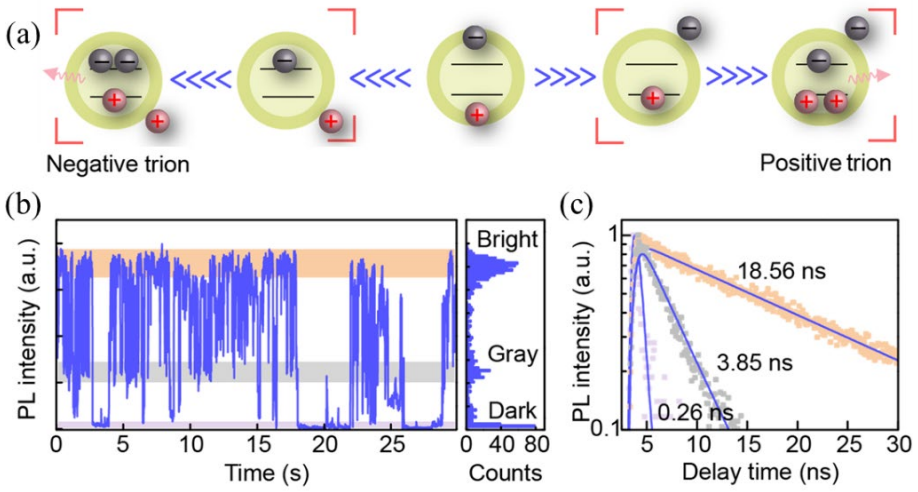

Figure 2 Auger-blinking. (a) Schematic diagram of the formation of positive and negative trion states. (b) Typical PL blinking trace of a single QD. Bright state, grey state, and dark state represent the neutral exciton state, negative trion state, and positive trion state, respectively. (c) Corresponding PL decay curves of bright state, grey state, and dark state. Reproduced with permission from Ref. [35], © American Chemical Society 2021.

bright state (on-state) and the dark state (off-state) occurs, and such a phenomenon is termed Auger-blinking. A typical Auger-blinking trajectory is displayed in Fig. 2(b), and the corresponding PL decay curves are presented in Fig. 2(c). In Auger-blinking of CdSe-based QDs, the PL intensity and lifetime of the positive trion states are often smaller than those of the negative trion states [35]. The reason is that the energy level density of hole states is much higher than that of electron states. As a result, the Auger process involving excitation within the hole band better satisfies the energy conservation requirements than the Auger process accompanied by electron excitation [36]. Recently, Qin and colleagues found that geometry-dependent dielectric screening can decrease Auger rates, and that positive trion states may encounter greater dielectric screening compared to the corresponding negative trion states [37]. By modifying the core–shell structure of the QDs to regulate the dielectric screening, they discovered that the PL intensity and lifetime of the negative and positive trion states were inverted [37, 38]. For perovskite QDs, positive and negative trion states are seldom differentiated in the PL trajectories [39–42]. This is because the effective masses of electrons and holes in perovskites are almost identical [41]. As a QD is charged with more charges, the carrier–carrier Coulomb interactions in the QD are enhanced, leading to changes in the Auger rate, the PL lifetime, and PL intensity. For instance, Lei et al. recently synthesized cube-shaped CdSe/CdS QDs [43]. The single cube-shaped CdSe/CdS QD exhibits multiple emission states, which have been attributed to neutral, singly-charged, doubly-charged, and triply-charged exciton states.

The BC-blinking of single QDs is usually described by the multiple recombination center (MRC) model [45]. The multiple recombination centers of QDs are non-radiative recombination centers made up of multiple surface defects, which can generate local energy levels located between QD's conduction and valence bands, as shown in Fig. 3(a). These local energy levels are known as surface trap states [46]. These surface trap states are capable of capturing the electron (or hole) in the exciton, which will then recombine non-radiatively with the opposite charge carrier in the QD core. The activation and deactivation of surface defects cause changes in the non-radiative recombination rate ($k_{nr}(t)$), leading to fluctuations in PL intensity ($I(t)$), that is, causing BC-blinking. A typical BC-blinking trajectory is displayed in Fig. 3(b). The BC-blinking can be mathematically expressed as $I(t) \propto k_r/(k_r + k_{nr}(t))$ [47], where k_r represents the radiative rate of single exciton. For BC-blinking trajectory, the radiative rate ratio among all the grey states is 1 [48]. The corresponding fluorescence lifetime-intensity distribution (FLID) displays a linear correlation between the PL intensity and the lifetime (Fig. 3(c)), which is in good agreement with the MRC model. The basic difference between BC-blinking and Auger-blinking is actually whether the radiation rate varies or not. The radiative rate of the BC-blinking remains constant. The changing of radiative rate in Auger-blinking results in a nonlinear relationship in the FLID [48].

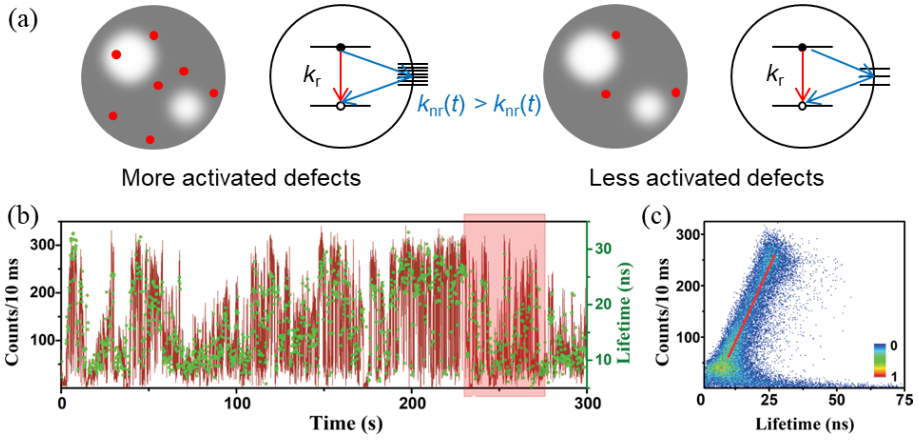

Figure 3 BC blinking. (a) Schematic diagram of the origin of BC-blinking. The red dots represent activated surface defects, the number of which is proportional to the non-radiative rate. (b) Typical BC-blinking trajectory of a single QD and corresponding lifetime values. (c) Corresponding FLID. Reproduced with permission from Ref. [44], © Tsinghua University Press 2022.

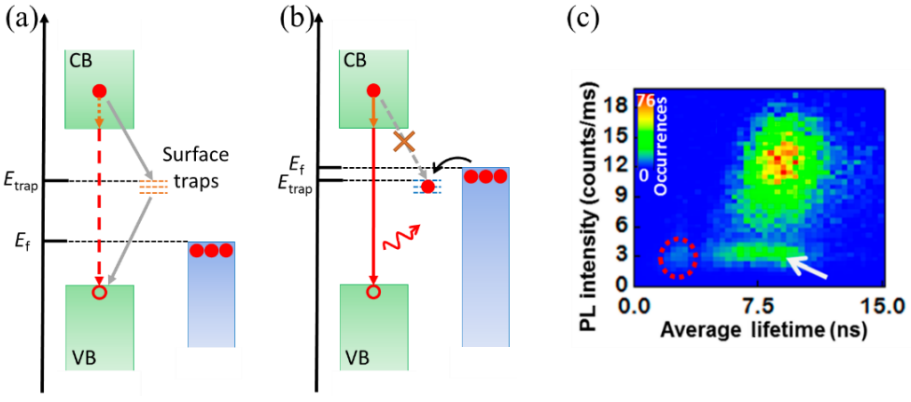

Figure 4 HC blinking. (a) and (b) Schematic diagram of the origin of HC-blinking. (a) Dim state arises from surface traps capturing hot electrons before they cool down to the conduction band edge. (b) Bright state occurs when the position of the E_F is above the energy of the surface traps (E_{trap}). (c) Typical FLID of a single QD. The dim state indicated by the arrow has the same lifetime as the bright state. Reproduced with permission from Ref. [50], © American Chemical Society 2019.

The HC-blinking behavior is similar to that of BC-blinking as it is also caused by surface trapping. However, it distinguishes from BC-blinking as the surface trap states can capture hot electrons and non-radiatively recombine with holes in the valence band, without capturing carriers at the band edge, as illustrated in Figs. 4(a) and 4(b). The capture of hot electrons does not reduce the PL lifetime, but rather only the PL intensity, as shown in Fig. 4(c). This type of non-radiative recombination does not compete with the radiative rate of band-edge excitons. Klimov and colleagues observed HC-blinking for the first time by regulating the Fermi level (E_F) of single QDs using spectroelectrochemistry [49]. However, the HC-blinking was rarely observed in most QDs, resulting in few subsequent reports [50, 51, 52].

Fluctuations in the PL intensity and lifetime of single QDs are often accompanied by changes in the PL spectrum. Wang and colleagues conducted low-temperature experiments to measure the PL spectrum of single perovskite QDs [42, 53], and found that the trion state spectrum was red-shifted compared to that of the single exciton state, as presented in Fig. 5. This phenomenon is attributable to differences in binding energy between the trion state and that of the single exciton state. Ihara and colleagues conducted a study in which they measured the PL properties of single CdSe/ZnS QDs at room temperature, and a surface charge-induced quantum-confined Stark effect was revealed through simultaneous measurements of PL intensity, lifetime, and spectrum [54]. The quantum confinement Stark effect is due to the localized electric field generated by the QD's surface charges, which alters the overlap of the electron and hole wave functions, as presented in Figs. 6(a) and 6(b). As the overlap between the electron and hole wave functions decreases, this can lead to a decrease in the radiative rate of QD excitons, ultimately resulting in an increase in the PL lifetime, a decrease in PL intensity, and a red shift in the spectrum. The study identified the quantum confinement Stark effect in perovskite single QDs by observing the phenomenon of reduced PL intensity (Fig. 6(c)) but extended lifetime (Fig. 6(d)) [55]. The inverse correlation between PL intensity and lifetime in FLID indicated by the red arrow further demonstrates the occurrence of the quantum confinement Stark effect (Fig. 6(e)). Moreover, it was observed that the surface charges of single QDs have the potential to modulate the fine energy level structure of QD band-edge excitons, hence changing the polarization of PL [16, 56].

3.2 Blinking control of single QDs

3.2.1 *Blinking control of single QDs by adjusting the light field*

The Auger-blinking of the single QDs is significantly affected by the excitation optical power density due to the formation of multi-

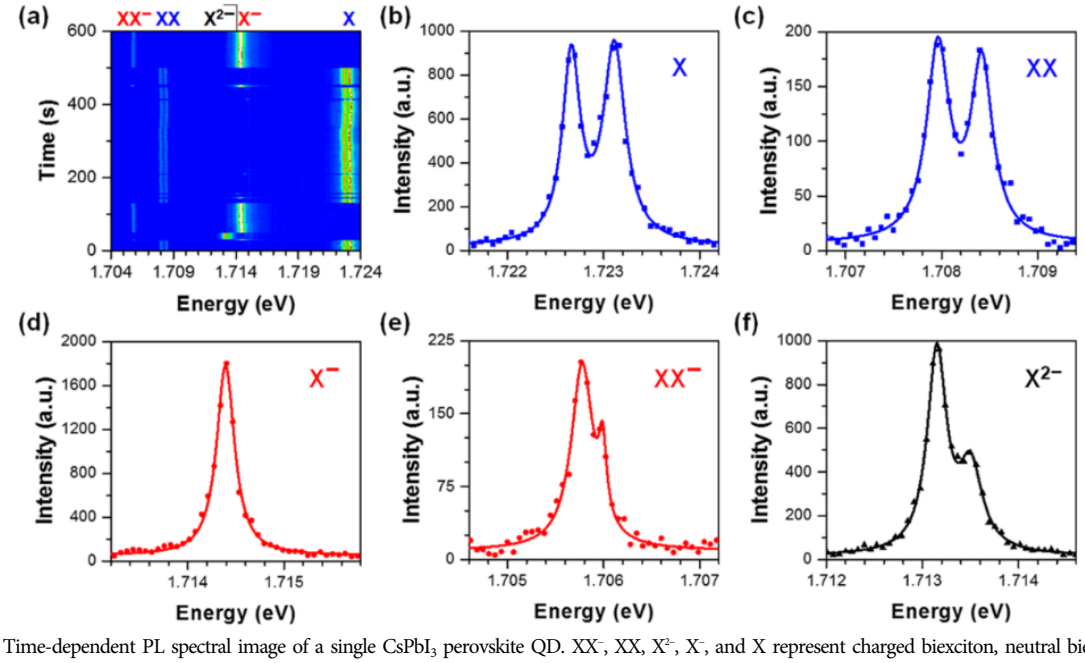

Figure 5 (a) Time-dependent PL spectral image of a single $CsPbI_3$ perovskite QD. XX^-, XX, X^{2-}, X^-, and X represent charged biexciton, neutral biexciton, doubly charged single exciton, singly charged single exciton, and neutral single exciton state, respectively. The PL spectra of X, XX, X^-, XX^-, and X^{2-} are plotted in (b)–(f), respectively. Reproduced with permission from Ref. [42], © American Physical Society 2017.

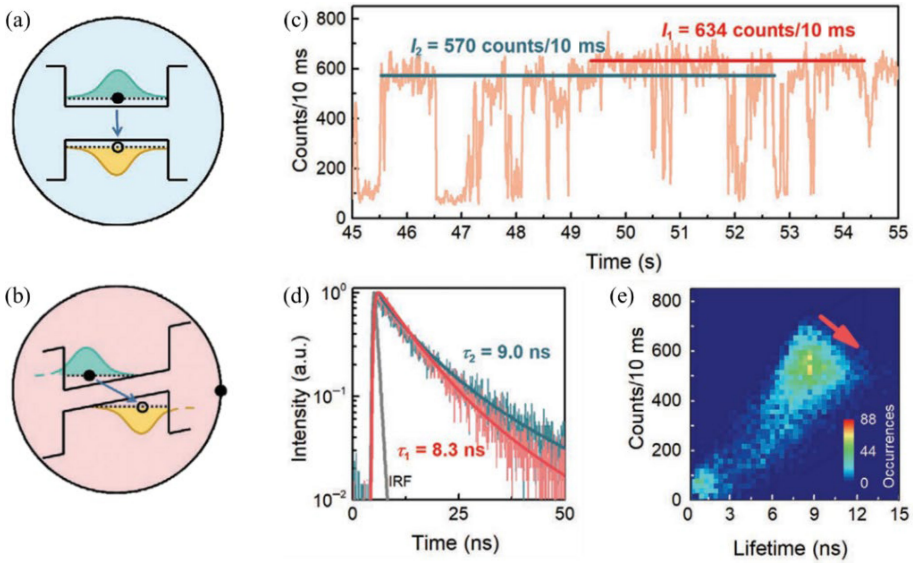

Figure 6 Intrinsic quantum-confined Stark effect of single $CH_3NH_3PbBr_3$ perovskite QDs. (a) Schematic illustration of a single exciton in the absence of a surface change. (b) Schematic illustration for the generation of quantum confinement Stark effect induced by a surface change. (c) Typical PL intensity trace for a single QD under the action of quantum confinement Stark effect. The PL intensity marked by red line and green line corresponding to normal single exciton state and quantum-confined Stark effect modified single exciton state, respectively. (d) Corresponding PL decay curves of the PL areas marked by red and green lines. The lower PL intensity trajectory has longer PL lifetimes. (e) Corresponding FLID map. Reproduced with permission from Ref. [55], © Wiley-VCH GmbH 2020.

excitons at higher excitation conditions [20, 57]. This is because the Auger recombination of multi-excitons may cause QD charging, as illustrated in Fig. 7(a) [33, 36, 58]. The QD charging can convert the bright state of PL intensity traces into the dim states. Thus far, the investigation of the blinking dynamics of various QDs has revealed that the blinking rate increases with the intensity of the excitation light, as depicted in Fig. 7(b) [33, 39, 53, 59]. Furthermore, the Auger-blinking is linked to the photon energy of the excitation light. The greater the photon energy of the excitation light, the more pronounced the PL blinking initiated by the Auger mechanism, as illustrated in Fig. 7(b) [19, 33]. We identified that the PL blinking of perovskite single QDs exhibits BC-blinking under weak light excitation conditions. However, both BC-blinking and Auger-blinking appear concurrently when the excitation light power increases [55, 60, 61]. Recently, conversion of PL blinking types has been observed in single colloidal QDs under higher excitation conditions [62]. The blinking behavior of single alloyed CdSe/ZnS QDs undergoes an irreversible conversion from Auger-blinking to BC-blinking, while single perovskite QDs exhibit reversible conversion between BC-blinking and more pronounced Auger-blinking.

3.2.2 *Blinking control of single QDs by adjusting the Fermi level*

The Fermi level can be adjusted by applying an external electric field to the single QDs. The elevated Fermi level has the ability to fill the trap states with electrons and suppress BC-blinking [49]. For Auger-blinking, when the Fermi level is adjusted above the conduction band, the single QD is more likely to be negatively

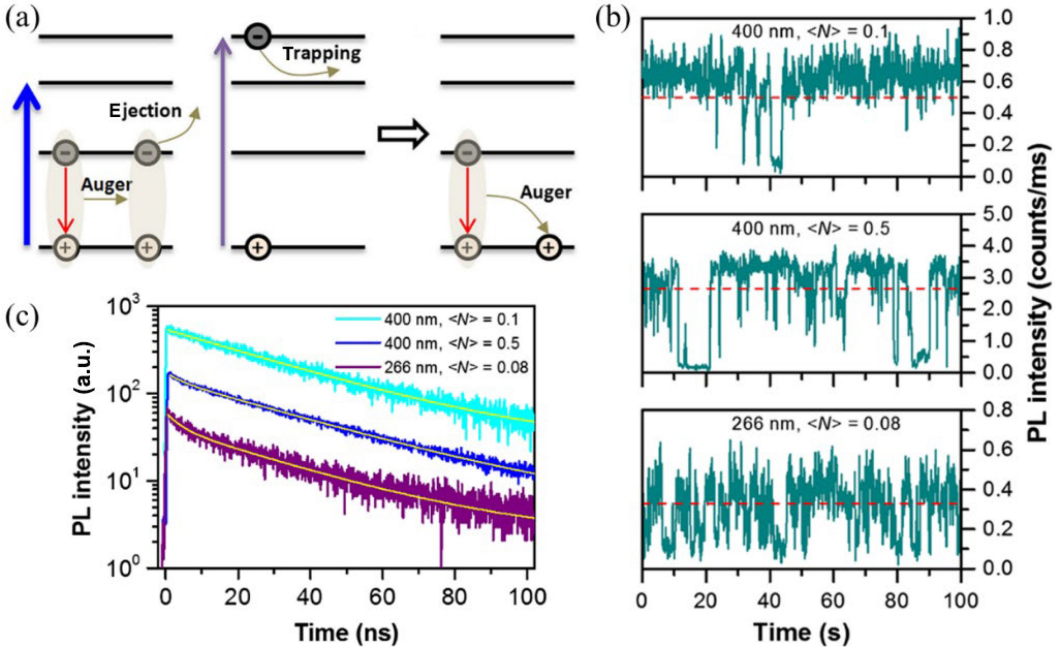

Figure 7 (a) Schematic illustration of charging process of QDs. (b) PL intensity traces of a single QD at different excitation conditions. The $\langle N \rangle$ in figure is the average number of photons absorbed per QD per pulse and is proportional to the power density of excitation light. Bright and dim states are separated by red dashed lines. (c) Corresponding PL decay curves of bright states. Biexciton lifetime is obtained by biexponential fitting. Reproduced with permission from Ref. [19], © American Physical Society 2016.

charged, leading to an increase in the proportion of dim states. By adjusting the electric field, Morozov et al. enabled the formation of highly charged exciton states consisting of 12 electrons and 1 hole within single QDs [63]. This results in an increased PL blinking of single QDs and an increase in the proportion of dim state in the PL intensity trajectory. LeBlanc et al. increased the proportion of dim state on the PL intensity trajectory by applying an electric field of 54 kV/cm across a single QD, which they attributed to increasing activated surface traps [64]. We achieved successful suppression of the PL blinking of single CdSeTe/ZnS QDs by encasing them within N-type semiconductor indium tin oxide (ITO) nanoparticles [65, 66]. We ascribe this achievement to the rise in the Fermi level, which prevents the electron transfers from the excited-state QDs to the trap states. We investigated the impact of surface charges on the blinking mechanisms of single CdSe/CdS/ZnS QDs by adjusting both positive and negative surface charges. It was discovered that positive surface charges can modify the blinking mechanisms of QDs from Auger-blinking to BC-blinking. The change is attributed to the positive surface charges which cause the surface traps to activate and deactivate, as shown in Fig. 8 [44].

3.2.3 Blinking control of single QDs by adjusting the core–shell structure

QDs with a core–shell structure exhibit higher PL emission stability than those with only a core. Gradual suppression of PL blinking was observed with the increase in shell thickness of core–shell QDs [59, 67–69]. This suppression can be attributed to the alleviation of biexciton Auger recombination, which induces the charging of QDs. Jain et al. [70] and Hou et al. [71] demonstrated that modifying the smoothness of the core–shell interface has no impact on the Auger recombination of CdSe-based QDs, and therefore has no influence on the Auger-blinking of single QDs. We found that single $Cd_xZn_{1-x}Se_yS_{1-y}$/ZnS QDs with a smooth core–shell interface potential exhibit more frequent blinking than those with a sharp core–shell interface potential, as illustrated in Fig. 9(a) [72]. We interpret this occurrence as electrons in excitons being more likely to delocalize towards the QD surface due to the smooth structure of the core–shell interface, resulting in their trapping by surface defects, as depicted in Fig. 9(b).

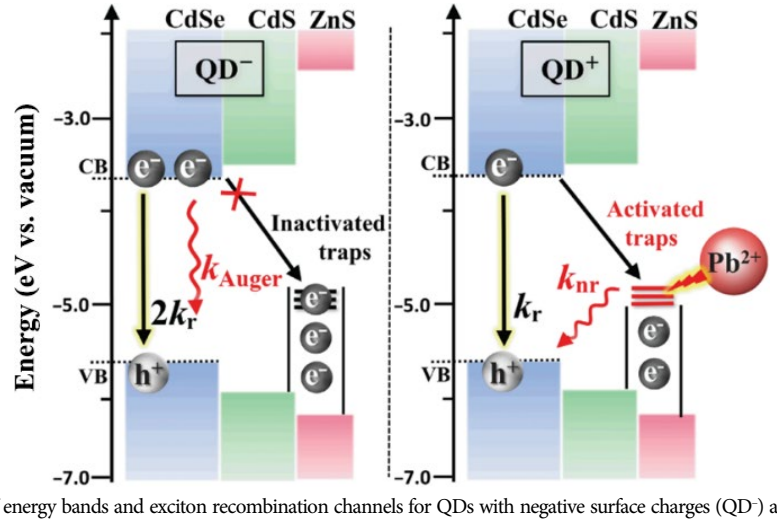

Figure 8 Schematic diagrams of energy bands and exciton recombination channels for QDs with negative surface charges (QD^-) and positive surface charges (QD^+), respectively. The negative surface charges passivate the surface traps of the QDs, while the positive surface charges will activate the surface traps to open the nonradiative recombination channels of excitons. Reproduced with permission from Ref. [44], © Tsinghua University Press 2022.

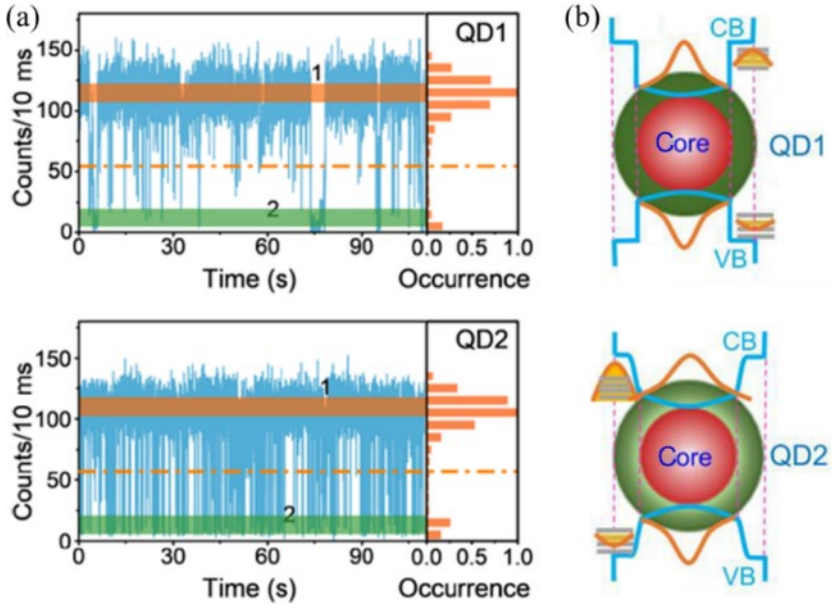

Figure 9 (a) Typical PL trajectories for single $Cd_xZn_{1-x}Se_yS_{1-y}$/ZnS core/shell QDs with sharp interface potential (QD1) and single QDs with smooth interface potential (QD2). The right panels show the corresponding PL intensity histograms. The PL blinking of QD2 is more frequent than that of QD1. (b) Schematic illustration of CB and VB of QD1 and QD2, respectively. The gray lines represent surface traps, and yellow shaded wave packets represent the ability of surface traps to capture carriers. Reproduced with permission from Ref. [72], © American Chemical Society 2020.

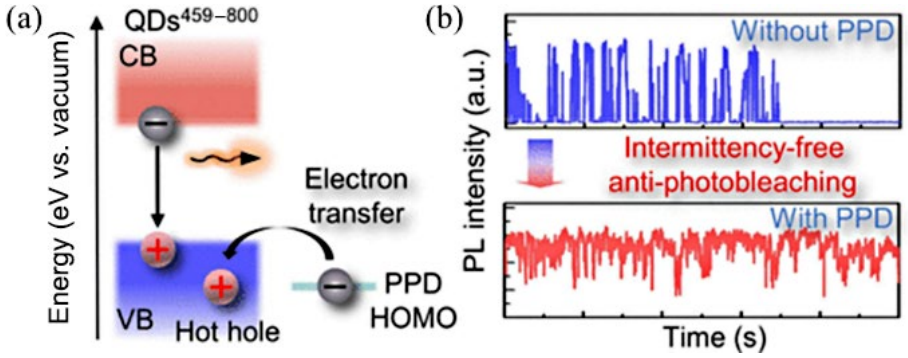

Figure 10 (a) Schematic diagrams of electron transfer from PPD molecules to positive trion of QDs, which accelerates QD discharging. (b) Suppression of the PL blinking of single CdSe-based QDs with PPD molecules. Reproduced with permission from Ref. [35], © American Chemical Society 2021.

3.2.4 Blinking control of single QDs by adjusting the charging and discharging rate

Charge transfer can accelerate the discharging process of single QDs, thereby suppressing their blinking. Hu et al. [73] investigated the effect of oxygen on the PL blinking of single QDs and discovered that the blinking frequency reduced as oxygen concentration increased in the air, because oxygen molecules provided additional discharging channels for the QDs through charge transfer. The successful suppression of PL blinking in various types of CdSe-based QDs was achieved through the use of p-phenylenediamine (PPD) molecules, as demonstrated in Fig. 10 [35, 74]. This was accomplished without affecting their PL intensity, lifetime, or emission spectra. PPD molecules function by transferring charges to eliminate redundant holes in QDs, resulting in the suppression of the long dark states generated by the positive trion state. Furthermore, the investigation revealed that PPD molecules successfully inhibit the photobleaching of CdSe-based QDs, extending the mean survival time of single QDs from a few minutes to over than 1 h. Moreover, PPD-stabilized QDs have been successfully implemented in multiple areas including single particle tracking and live cell imaging. Another amine compound, dimethylaniline (DMA) molecule, was employed by Thomas et al. [75] to effectively suppress the PL blinking of CdSe/ZnS core–shell QDs. They also managed to suppress the PL blinking of perovskite single QDs by filling the surface defects through the introduction of CH_3NH_3Br and CH_3NH_3I halide precursors [76].

4 Multiexciton recombination dynamics of single QDs

4.1 Measurement of multiexciton emission properties of single QDs

4.1.1 Measurement of biexciton lifetime for single QDs

The biexciton lifetime of single QDs is typically an order of magnitude shorter than that of single exciton. On the one hand, the radiative lifetime of biexciton is one-fourth that of single exciton, because the radiative recombination path of biexciton state is four times that of a single exciton state, as depicted in Fig. 11. This ratio of radiative recombination path is often used for estimating the radiative lifetime of biexcitons [39]. In contrast, the nonradiative lifetime of biexciton due to Auger decay is a quarter that of the trion state, presuming that the positive and negative trion states possess the same Auger lifetime. When fitting the PL decay curve of a single QD with a bi-exponential function, the shorter lifetime is due to biexciton emission and the longer lifetime is due to single exciton emission. Huang et al. obtained the biexciton lifetime through biexponential fitting the PL decay curve of bright state in single QD's intensity trajectory, as depicted in Fig. 7(c), avoiding the trion states' influence on biexciton lifetime measurements by extracting bright-state photons from intensity trajectories [19, 77]. Single-QD spectroscopy combined with HBT analysis offers a novel means of determining the biexciton lifetimes. A two-photon event is formed by the cascaded

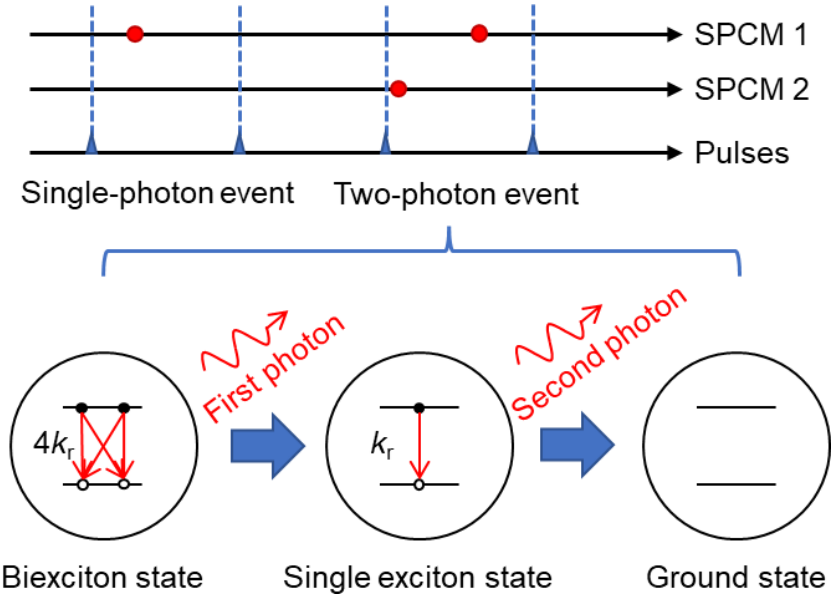

Figure 11 Schematic diagram of single-photon event, two-photon event, and cascaded relaxation of biexciton state to the ground state.

relaxation of the biexciton state to the ground state: The first photon is emitted when transitioning from the biexciton state to the single exciton state, and the second photon is emitted when transitioning from the single exciton state to the ground state, as depicted in Fig. 11. By extracting the first photons from the two-photon events to construct a biexciton decay curve and fitting it with a single exponent, the biexciton lifetime can be obtained [36].

4.1.2 *Measurement of biexciton quantum yield for single QDs*

Based on the HBT experimental scheme, Bawendi and colleagues developed a method to measure the biexciton quantum yield of single QDs using second-order correlation function ($g^{(2)}(\tau)$) [78]. Under weak light excitation conditions, the ratio of the quantum yields of the biexciton to the single exciton is approximately equal to the ratio of the central peak's area to the side peak's area in the $g^{(2)}(\tau)$ function (denoted by R). This method has been widely used for determining biexciton quantum yield. Htoon and colleagues analyzed the $g^{(2)}(\tau)$ of different intensity regions on the PL intensity trajectory [79]. They observed an increase in the R value as the PL intensity decreased. This is due to the fact that the single exciton quantum yield, which serves as the denominator of R, is roughly proportional to the PL intensity. Chen and colleagues employed a comparable methodology to measure the $g^{(2)}(\tau)$ function across various intensity regions. The results showed a smaller R value for the neutral exciton state than for the negative trion state and positive trion states [80].

We have developed a time- and intensity-resolved single-photon statistical method [81]. This method can directly measure the quantum yield of biexcitons, independent of the quantum yield of single excitons, and allows higher excitation conditions. Through this method, we determined the evolution characteristics of the biexciton quantum yield of single QDs with PL intensity for BC-blinking and Auger-blinking trajectories. Further, we revealed that at the single-QD level, the ratios of radiative and nonradiative rates between charged and neutral biexcitons in Auger-blinking are consistent with the asymmetric band structure theoretical expectations (Figs. 12(a) and 12(b)). Furthermore, the research discovered that surface traps of QDs could offer non-radiative recombination channels for biexcitons. Experimental measurements show that this surface's non-radiative recombination rate for biexcitons is roughly 4 times that of single excitons, as depicted in Figs. 12(c) and 12(d).

4.1.3 *Measurement of biexciton spectrum for single QDs*

At room temperature, the biexciton spectrum of a single QD typically blends with the spectra of single exciton and trion state, making it challenging to distinguish [82]. Consequently, low temperature experimental conditions are necessary to measure the biexciton spectrum of single QD. Wang and colleagues [42] conducted an analysis of the biexciton spectrum of single perovskite QDs at low temperatures and determined the impact of QD charging on the fine energy level structure of biexcitons by measuring the spectrum changes in real time with the intensity of PL. The results are presented in Fig. 5. In order to obtain room temperature measurements of biexciton spectrum for a single QD, Vonk et al. [83] developed a cascade spectroscopy method. This method allows for the resolution of the photon energy of the first or second photon in two-photon events by incorporating a galvo

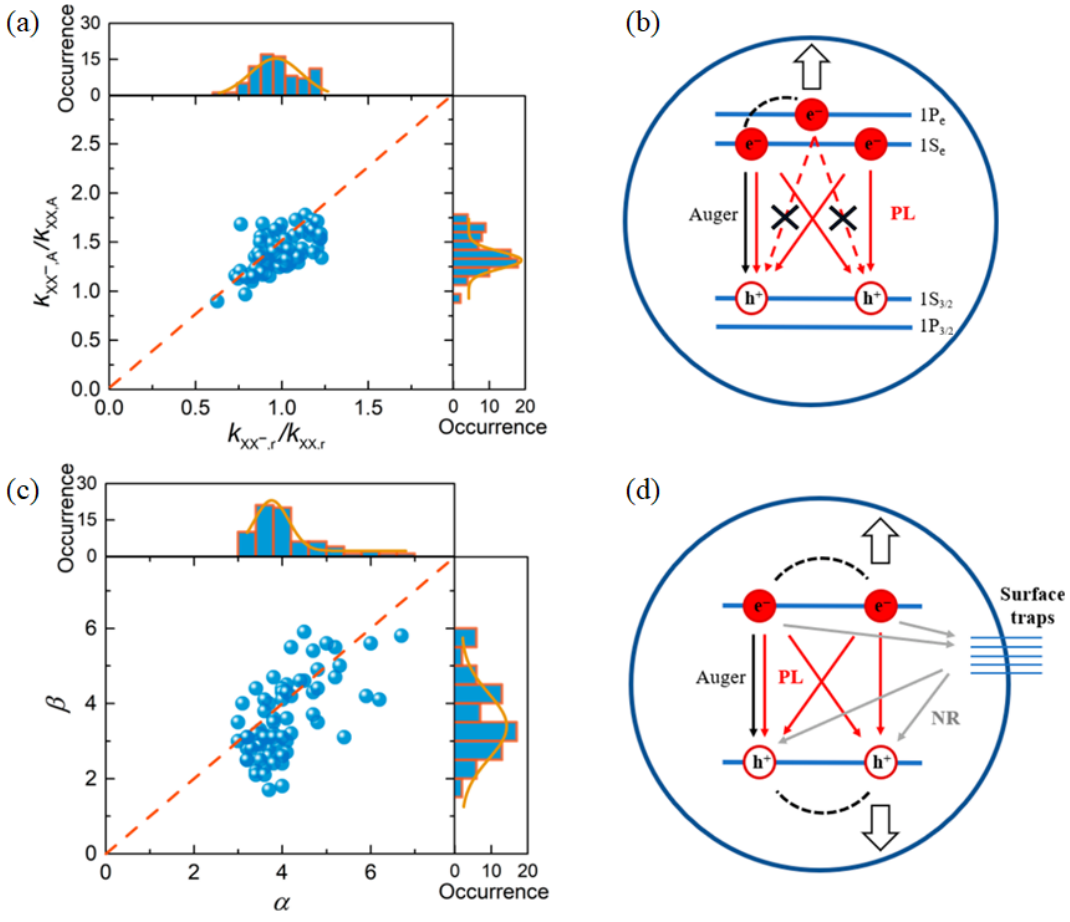

Figure 12 (a) Statistical distribution of the ratios of radiative rates and of Auger rates between charged and neutral biexciton states. (b) Schematic of radiative recombination pathways (red arrows) and nonradiative Auger recombination (black arrows) of the charged biexciton state for a CdSe-based QD. (c) Statistical distributions of the radiative rate ratio (α) and of the surface nonradiative rate ratio (β) between biexciton and single exciton. (d) Schematic of radiative recombination pathways (red arrows), Auger recombination pathway (black arrows), and surface nonradiative recombination pathways (gray arrows) for the biexciton state. Reproduced with permission from Ref. [81], © American Chemical Society 2020.

mirror and transmission grating in the HBT optical path. The method is similar to the first photon method for measuring biexciton lifetime [36]. The biexciton spectrum was acquired by extracting the first arriving photon in the time sequence of biexciton and single exciton radiation. The biexciton spectrum of the single QDs disclosed an average spectral line width of 86 meV. Lubin et al. [84] developed a heralded spectroscopy using a single-photon avalanche diode array-based spectrometer, enabling direct observation of biexciton–exciton emission cascades and measurement of the biexciton binding energy of single QDs at room temperature.

4.2 Manipulation of biexciton emission properties of single QDs

4.2.1 Biexciton emission of single QDs under different interface environments

The $g^{(2)}(\tau)$ function of CdSeTe/ZnS single QDs on N-type semiconductor ITO nanoparticles was measured, revealing that the R value of single QDs on ITO was significantly higher than that on glass coverslips. This suggests that the ratio of the quantum yield of biexciton to single exciton is increased on ITO [85]. Rakovich and colleagues [86] adjusted the distance between the single QDs and the gold nanoparticle film by varying the thickness of the polymethyl methacrylate (PMMA) polymer film, and found that the R value rises with declining PMMA thickness, as shown in Fig. 13(a). Masuo et al. [87] employed the tip of an atomic force microscopy (AFM) to bring a cubic gold nanoparticle in close proximity to CdSe/ZnS single QDs. The measured R value increases with the reduced distances, as illustrated in Fig. 13(b). The observed increase in the R value can be accounted for by the joint effect of fluorescence resonance energy transfer between QDs and gold nanoparticles, and the Purcell effect.

4.2.2 Effect of QD core–shell structure on biexciton

Naiki et al. [88], Hiroshige et al. [89], and Rabouw et al. [90] altered the Auger recombination rate of the biexciton by regulating the shell thickness of the QDs. Ma et al. [91] and Mangum et al. [92] modified the Auger recombination rate of the biexciton by regulating the size of the QD core. Park et al. [93] and Hou et al. [71] modified the Auger recombination rate of the biexciton by adding an alloy layer between the core–shell of QDs in order to adjust the core–shell interface potential. Additionally, Vaxenburg et al. [58] calculated the fine energy level structure of biexcitons based on the asymmetric energy level structure and hole–hole interaction of QDs and theoretically simulated the effects of core size of QD and shell thickness on the Auger recombination rate of the biexciton. Our discovery reveals that the smooth core–shell interface potential can slightly reduce the Auger recombination of biexcitons in single QDs. The reason for this is that the smooth interfacial potential can increase the delocalization of the electron wave function and therefore reduce the Auger recombination rate of biexcitons [72].

4.2.3 Application of time-gating technique to exciton recombination dynamics of single QDs

The PL lifetime of multi-excitons is much shorter than that of single exciton due to the Auger effect. Hence, configuring a time gate on the single-photon detector can effectively eliminate the multi-exciton emission. Mangum et al. [94] successfully disentangled the effects of clustering and multi-exciton emission of QDs to distinguish individual QDs from QD clusters using time-gating technique [95, 96]. Feng et al. [97] used an acousto-optic modulator as a time-delay gate setting to filter out the multi-exciton emission of single QDs under high-power excitation in the detection optical path of a confocal microscope and achieved a high-purity single-photon source at room temperature. The time-gating technique was combined with the spatially coincident single-photon statistical technique [98], enabling rapid and precise identification of single QDs during the scanning process of the confocal microscope [99]. The time-gating technique successfully identified single QDs on monolayer MoS_2, despite the spectral overlap between the intense emission of MoS_2 and the weak emission of single QDs, as illustrated in Fig. 14 [100].

5 Summary and outlook

Single-QD spectroscopy has shown considerable advantages and potential for the measurement and characterization of photophysical properties of QD materials. As new functional QD materials continue to be developed, it is crucial to enhance single-QD spectroscopy for more accurate optical measurements and characterization.

Single-QD spectroscopy typically requires the use of confocal microscopy to measure numerous single QDs one by one in order to obtain statistical results, which can be a time-intensive process. Therefore, it is important to devise a method to measure multiple single QDs simultaneously to improve measurement efficiency.

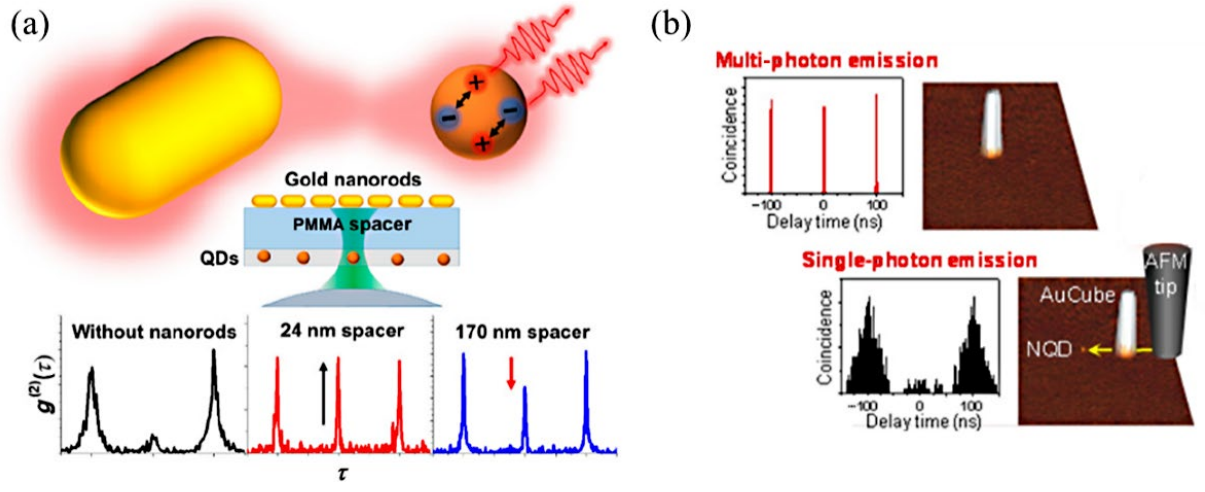

Figure 13 (a) Manipulating biexciton emission of single QDs using gold nanorods. Their distance was adjusted by PMMA film thickness, and the $g^{(2)}(\tau)$ function was used to characterize the biexciton emission. Reproduced with permission from Ref. [86], © American Chemical Society 2019. (b) Biexciton emission enhancement from a single QD using AFM manipulation of a cubic gold nanoparticle. Reproduced with permission from Ref. [87], © American Chemical Society 2015.

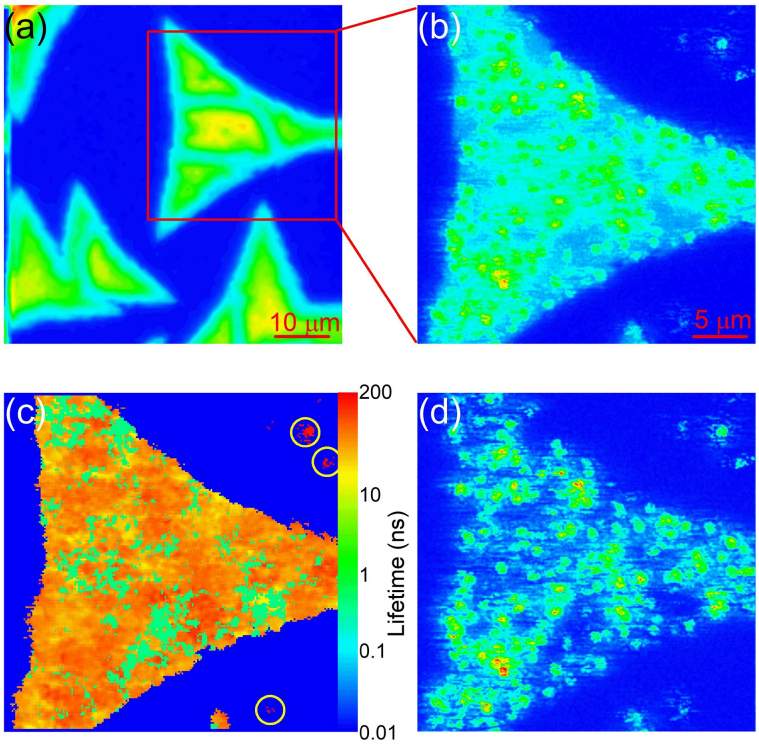

Figure 14 PL intensity images of single QDs on monolayer MoS_2 with long-pass filters of (a) 655 nm and (b) 736 nm. (c) Corresponding PL lifetime images with the long-pass filter of 736 nm. The areas marked by yellow circles are single QDs on silicon. (d) Corresponding time-gated PL intensity image with delay time of 5 ns and the emission filter of 736 nm. Reproduced with permission from Ref. [100], © The Owner Societies 2023.

For instance, the method of wide-field fluorescence imaging enables the simultaneous measurement of PL blinking dynamics of tens or even hundreds of single QDs [101–103]. Houel et al. [104] presented a method for deriving the power-law exponents from the single QDs' intensity autocorrelation functions. This is achieved through simultaneous recording of the emission time trajectories of 450 single QDs, rather than the commonly used threshold method. Furthermore, the defocusing method can also simultaneously acquire the dipole orientation information of large numbers of single particles [56, 105, 106]. Analyzing the PL dynamics of numerous single QDs frequently necessitates the use of more sophisticated data analysis methods, like machine learning.

Measuring the absolute quantum yield of a single QD remains a challenging task due to limitations in efficiently determining the number of photons absorbed by a single QD. As an alternative approach, the radiative rate and non-radiative rate of the single QD, which determine the PL quantum yield of QDs, can be measured. By making adjustments of the radiation rate and observing changes in the total rate (i.e., the reciprocal of the PL lifetime), the absolute quantum yield of the single QD can be inferred [32]. However, achieving quantitative changes in the radiative rate of a single QD while maintaining constant non-radiative rate is challenging in conventional experimental systems. Thus, it is imperative to devise a more efficient and concise method for determining the absolute quantum yield of single QDs through single-QD spectroscopy.

To examine the influence of QD materials' structural properties on their PL dynamics, it is essential to develop a technology that combines single-QD spectroscopy with other measurement methods. For instance, Tachikawa et al. [107] merged high-resolution electron microscopy with single-QD spectroscopy to acquire the correlation features of single QD morphology and PL dynamics. Tian et al. [108] demonstrated the carrier diffusion process in single crystals through the integration of PL scanning imaging microscopy with time-resolved technology. In the future, the trend in development will encompass the use of single-QD spectroscopy combined with other measurement methods.

Single QDs can be used to prepare both single photon sources and entangled photon sources, which play an extremely important role in quantum information [23, 109, 110]. The process of quantum information demands that single QDs produce indistinguishable single photons or entangled photon pairs, and necessitates that the optical coherence time surpasses twice the lifetime of its spontaneous emission. Bawendi and colleagues [111, 112] discovered that at low temperature, red-emitting InP/ZnSe/ZnS colloidal QDs have narrower line widths than typically synthesized CdSe QDs. Additionally, InP/ZnSe/ZnS single QDs exhibit single-photon purities $g^{(2)}(0)$ of 0.077–0.086 and a lower-bounded optical coherence time of 250 ps. Utzat et al. [113] found that perovskite single QDs exhibit highly efficient single-photon emission with optical coherence times of up to 80 ps, which is a significant portion of their radiative lifetime of 210 ps. Lv et al. [114] found that an external electric field can eliminate the fine energy level structures of single exciton and biexciton of single perovskite QDs at low temperature. This discovery could pave the way for the generation of polarization-entangled photon pairs.

Currently, single-QD spectroscopy has proven to be a valuable technical tool, demonstrating numerous advantages and potential in solving scientific problems across various disciplines. The advancement of single-QD spectroscopy technology will continue to make substantial contributions to various disciplines, leading to further advancements and breakthroughs in the future.

Ackowledgements

This work was supported by the National Key Research and Development Program of China (No. 2022YFA1404201), the National Natural Science Foundation of China (Nos. 62305201, 62075120, 62075122, 62127817, 62222509, U22A2091, U23A20380, and 62105193), Program for Changjiang Scholars

and Innovative Research Team (No. IRT_17R70), Shanxi Province Science and Technology Major Special Project (No. 202201010101005), Fundamental Research Program of Shanxi Province (Nos. 202103021223254 and 202203021221121), Graduate Innovation Project in Shanxi Province (No. 2023KY460), Shanxi Province Science and Technology Innovation Talent Team (No. 202204051001014), Science and Technology Cooperation Project of Shanxi Province (No. 202104041101021), and Shanxi "1331 Project", 111 projects (No. D18001).

References

[1] Pietryga, J. M.; Park, Y. S.; Lim, J.; Fidler, A. F.; Bae, W. K.; Brovelli, S.; Klimov, V. I. Spectroscopic and device aspects of nanocrystal quantum dots. *Chem. Rev.* **2016**, *116*, 10513–10622.

[2] Efros, A. L.; Nesbitt, D. J. Origin and control of blinking in quantum dots. *Nat. Nanotechnol.* **2016**, *11*, 661–671.

[3] García de Arquer, F. P.; Talapin, D. V.; Klimov, V. I.; Arakawa, Y.; Bayer, M.; Sargent, E. H. Semiconductor quantum dots: Technological progress and future challenges. *Science* **2021**, *373*, eaaz8541.

[4] Kagan, C. R.; Lifshitz, E.; Sargent, E. H.; Talapin, D. V. Building devices from colloidal quantum dots. *Science* **2016**, *353*, aac5523.

[5] Carey, G. H.; Abdelhady, A. L.; Ning, Z. J.; Thon, S. M.; Bakr, O. M.; Sargent, E. H. Colloidal quantum dot solar cells. *Chem. Rev.* **2015**, *115*, 12732–12763.

[6] Lin, Y. H.; Sakai, N.; Da, P. M.; Wu, J. Y.; Sansom, H. C.; Ramadan, A. J.; Mahesh, S.; Liu, J. L.; Oliver, R. D. J.; Lim, J. et al. A piperidinium salt stabilizes efficient metal-halide perovskite solar cells. *Science* **2020**, *369*, 96–102.

[7] Bao, J.; Bawendi, M. G. A colloidal quantum dot spectrometer. *Nature* **2015**, *523*, 67–70.

[8] Liu, L. G.; Deng, L. G.; Huang, S.; Zhang, P.; Linnros, J.; Zhong, H. Z.; Sychugov, I. Photodegradation of organometal hybrid perovskite nanocrystals: Clarifying the role of oxygen by single-dot photoluminescence. *J. Phys. Chem. Lett.* **2019**, *10*, 864–869.

[9] Krieg, F.; Ong, Q. K.; Burian, M.; Rainò, G.; Naumenko, D.; Amenitsch, H.; Süess, A.; Grotevent, M. J.; Krumeich, F.; Bodnarchuk, M. I. et al. Stable ultraconcentrated and ultradilute colloids of $CsPbX_3$ (X = Cl, Br) nanocrystals using natural lecithin as a capping ligand. *J. Am. Chem. Soc.* **2019**, *141*, 19839–19849.

[10] Kaur, G.; Babu, K. J.; Ghorai, N.; Goswami, T.; Maiti, S.; Ghosh, H. N. Polaron-mediated slow carrier cooling in a type-1 3D/0D $CsPbBr_3$@Cs_4PbBr_6 core–shell perovskite system. *J. Phys. Chem. Lett.* **2019**, *10*, 5302–5311.

[11] Wu, R. X.; Luo, J. J.; Guo, X. J.; Wang, X. S.; Ma, Z. H.; Li, B.; Cheng, L. Y.; Miao, X. Y. Phosphorescence quenching study of Cu(II)-ions-induced Mn-doped ZnS quantum dots revealed by intensity- and lifetime-resolved spectroscopy. *Chem. Phys. Lett.* **2021**, *781*, 138960.

[12] Fan, Q. X.; Yan, Z.; Zhou, H.; Yao, Y. G.; Wang, Z. K.; Gao, Y. N.; Wang, Y. L.; Lu, S. B.; Liu, M.; Ji, W. Near-infrared multiphoton absorption and third harmonic generation with $CsPbBr_3$ quantum dots embedded in micro-particles of metal-organic frameworks. *J. Mater. Chem. C* **2023**, *11*, 5788–5795.

[13] Zhou, J. J.; Chizhik, A. I.; Chu, S.; Jin, D. Y. Single-particle spectroscopy for functional nanomaterials. *Nature* **2020**, *579*, 41–50.

[14] Bai, X. Q.; Li, H. Y.; Peng, Y. G.; Zhang, G. F.; Yang, C. G.; Guo, W. L.; Han, X.; Li, J. L.; Chen, R. Y.; Qin, C. B. et al. Role of aspect ratio in the photoluminescence of single CdSe/CdS dot-in-rods. *J. Phys. Chem. C* **2022**, *126*, 2699–2707.

[15] Liang, X. L.; Qin, C. B.; Qiao, Z. X.; Kang, W. H.; Yin, H. L.; Dong, S.; Li, X. D.; Wang, S.; Su, X. L.; Zhang, G. F. et al. Optical interference effect in the hybrid quantum dots/two-dimensional materials: Photoluminescence enhancement and modulation. *Opt. Express* **2022**, *30*, 26557–26569.

[16] Zhang, G. F.; Yang, C. G.; Ge, Y.; Peng, Y. G.; Chen, R. Y.; Qin, C. B.; Gao, Y.; Zhang, L.; Zhong, H. Z.; Zheng, Y. J. et al. Influence of surface charges on the emission polarization properties of single CdSe/CdS dot-in-rods. *Front. Phys.* **2019**, *14*, 63601.

[17] Rabouw, F. T.; de Mello Donega, C. Excited-state dynamics in colloidal semiconductor nanocrystals. *Top. Curr. Chem.* **2016**, *374*, 58.

[18] Yao, Y. G.; Zhu, Y. K.; Hu, A.; Gao, Y. N. Temperature-regulated in-plane exciton dynamics in CdSe/CdSeS colloidal quantum well heterostructures. *ACS Photonics* **2023**, *10*, 4052–4060.

[19] Hu, F. R.; Lv, B. H.; Yin, C. Y.; Zhang, C. F.; Wang, X. Y.; Lounis, B.; Xiao, M. Carrier multiplication in a single semiconductor nanocrystal. *Phys. Rev. Lett.* **2016**, *116*, 106404.

[20] Ihara, T. Biexciton cascade emission reveals absolute absorption cross section of single semiconductor nanocrystals. *Phys. Rev. B* **2016**, *93*, 235442.

[21] Senellart, P.; Solomon, G.; White, A. High-performance semiconductor quantum-dot single-photon sources. *Nat. Nanotechnol.* **2017**, *12*, 1026–1039.

[22] Klimov, V. I. Multicarrier interactions in semiconductor nanocrystals in relation to the phenomena of Auger recombination and carrier multiplication. *Annu. Rev. Condens. Matter Phys.* **2014**, *5*, 285–316.

[23] Schimpf, C.; Reindl, M.; Huber, D.; Lehner, B.; Covre Da Silva, S. F.; Manna, S.; Vyvlecka, M.; Walther, P.; Rastelli, A. Quantum cryptography with highly entangled photons from semiconductor quantum dots. *Sci. Adv.* **2021**, *7*, eabe8905.

[24] Cui, J.; Beyler, A. P.; Bischof, T. S.; Wilson, M. W. B.; Bawendi, M. G. Deconstructing the photon stream from single nanocrystals: From binning to correlation. *Chem. Soc. Rev.* **2014**, *43*, 1287–1310.

[25] Efros, A. L.; Rosen, M. Random telegraph signal in the photoluminescence intensity of a single quantum dot. *Phys. Rev. Lett.* **1997**, *78*, 1110–1113.

[26] Nirmal, M.; Dabbousi, B. O.; Bawendi, M. G.; Macklin, J. J.; Trautman, J. K.; Harris, T. D.; Brus, L. E. Fluorescence intermittency in single cadmium selenide nanocrystals. *Nature* **1996**, *383*, 802–804.

[27] Han, S. P.; Qin, C. B.; Song, Y. R.; Dong, S.; Lei, Y.; Wang, S.; Su, X. L.; Wei, A. N.; Li, X. D.; Zhang, G. F. et al. Photostable fluorescent molecules on layered hexagonal boron nitride: Ideal single-photon sources at room temperature. *J. Chem. Phys.* **2021**, *155*, 244301.

[28] Li, B.; Zhang, G. F.; Chen, R. Y.; Qin, C. B.; Hu, J. Y.; Xiao, L. T.; Jia, S. T. Research progress of single quantum-dot spectroscopy and exciton dynamics. *Acta Phys. Sin.* **2022**, *71*, 067802.

[29] Chen, R. Y.; Xia, B.; Zhou, W. J.; Zhang, G. F.; Qin, C. B.; Hu, J. Y.; Scheblykin, I. G.; Xiao, L. T. Environment-dependent metastable nonradiative recombination centers in perovskites revealed by photoluminescence blinking. *Adv. Photonics Res.* **2022**, *3*, 2100271.

[30] Nazir, Z.; Lun, Y.; Li, J. L.; Yang, G. L.; Liu, M. R.; Li, S. Q.; Tang, G.; Zhang, G. F.; Hong, J. W.; Xiao, L. T. et al. Breaking the symmetry of colloidal 2D nanoplatelets: Twist induced quantum coupling. *Nano Res.* **2023**, *16*, 10522–10529.

[31] Chen, R. Y.; Xia, B.; Zhou, W. J.; Guan, W. L.; Zhang, G. F.; Qin, C. B.; Hu, J. Y.; Xiao, L. T.; Jia, S. T. Underestimated effect of the polymer encapsulation process on the photoluminescence of perovskite revealed by *in situ* single-particle detection. *Opt. Express* **2021**, *29*, 1851–1869.

[32] Brokmann, X.; Coolen, L.; Dahan, M.; Hermier, J. P. Measurement of the radiative and nonradiative decay rates of single CdSe nanocrystals through a controlled modification of their spontaneous emission. *Phys. Rev. Lett.* **2004**, *93*, 107403.

[33] Meng, R. Y.; Qin, H. Y.; Niu, Y.; Fang, W.; Yang, S.; Lin, X.; Cao, H. J.; Ma, J. L.; Lin, W. Z.; Tong, L. M. et al. Charging and discharging channels in photoluminescence intermittency of single colloidal CdSe/CdS core/shell quantum dot. *J. Phys. Chem. Lett.* **2016**, *7*, 5176–5182.

[34] Qin, H. Y.; Meng, R. Y.; Wang, N.; Peng, X. G. Photoluminescence intermittency and photo-bleaching of single colloidal quantum dot. *Adv. Mater.* **2017**, *29*, 1606923.

[35] Yang, C. G.; Xiao, R. L.; Zhou, S. R.; Yang, Y. G.; Zhang, G. F.; Li, B.; Guo, W. L.; Han, X.; Wang, D. H.; Bai, X. Q. et al. Efficient, stable, and photoluminescence intermittency-free CdSe-based quantum dots in the full-color range. *ACS Photonics* **2021**, *8*, 2538–2547.

[36] Park, Y. S.; Bae, W. K.; Pietryga, J. M.; Klimov, V. I. Auger recombination of biexcitons and negative and positive trions in individual quantum dots. *ACS Nano* **2014**, *8*, 7288–7296.
[37] Hou, X. Q.; Kang, J.; Qin, H. Y.; Chen, X. W.; Ma, J. L.; Zhou, J. H.; Chen, L. P.; Wang, L. J.; Wang, L. W.; Peng, X. G. Engineering Auger recombination in colloidal quantum dots via dielectric screening. *Nat. Commun.* **2019**, *10*, 1750.
[38] Hou, X. Q.; Qin, H. Y.; Peng, X. G. Enhancing dielectric screening for Auger suppression in CdSe/CdS quantum dots by epitaxial growth of ZnS shell. *Nano Lett.* **2021**, *21*, 3871–3878.
[39] Park, Y. S.; Guo, S. J.; Makarov, N. S.; Klimov, V. I. Room temperature single-photon emission from individual perovskite quantum dots. *ACS Nano* **2015**, *9*, 10386–10393.
[40] Yarita, N.; Tahara, H.; Ihara, T.; Kawawaki, T.; Sato, R.; Saruyama, M.; Teranishi, T.; Kanemitsu, Y. Dynamics of charged excitons and biexcitons in $CsPbBr_3$ perovskite nanocrystals revealed by femtosecond transient-absorption and single-dot luminescence spectroscopy. *J. Phys. Chem. Lett.* **2017**, *8*, 1413–1418.
[41] Becker, M. A.; Vaxenburg, R.; Nedelcu, G.; Sercel, P. C.; Shabaev, A.; Mehl, M. J.; Michopoulos, J. G.; Lambrakos, S. G.; Bernstein, N.; Lyons, J. L. et al. Bright triplet excitons in caesium lead halide perovskites. *Nature* **2018**, *553*, 189–193.
[42] Yin, C. Y.; Chen, L. Y.; Song, N.; Lv, Y.; Hu, F. R.; Sun, C.; Yu, W. W.; Zhang, C. F.; Wang, X. Y.; Zhang, Y. et al. Bright-exciton fine-structure splittings in single perovskite nanocrystals. *Phys. Rev. Lett.* **2017**, *119*, 026401.
[43] Lei, H. X.; Liu, S. J.; Li, J. Z.; Li, C. Y.; Qin, H. Y.; Peng, X. G. Band-edge energy levels of dynamic excitons in cube-shaped CdSe/CdS core/shell nanocrystals. *ACS Nano* **2023**, *17*, 21962–21972.
[44] Li, J. L.; Wang, D. F.; Zhang, G. F.; Yang, C. G.; Guo, W. L.; Han, X.; Bai, X. Q.; Chen, R. Y.; Qin, C. B.; Hu, J. Y. et al. The role of surface charges in the blinking mechanisms and quantum-confined stark effect of single colloidal quantum dots. *Nano Res.* **2022**, *15*, 7655–7661.
[45] Frantsuzov, P. A.; Volkán-Kacsó, S.; Jankó, B. Model of fluorescence intermittency of single colloidal semiconductor quantum dots using multiple recombination centers. *Phys. Rev. Lett.* **2009**, *103*, 207402.
[46] Frantsuzov, P. A.; Marcus, R. A. Explanation of quantum dot blinking without the long-lived trap hypothesis. *Phys. Rev. B* **2005**, *72*, 155321.
[47] Podshivaylov, E. A.; Kniazeva, M. A.; Tarasevich, A. O.; Eremchev, I. Y.; Naumov, A. V.; Frantsuzov, P. A. A quantitative model of multi-scale single quantum dot blinking. *J. Mater. Chem. C* **2023**, *11*, 8570–8576.
[48] Yuan, G. C.; Gómez, D. E.; Kirkwood, N.; Boldt, K.; Mulvaney, P. Two mechanisms determine quantum dot blinking. *ACS Nano* **2018**, *12*, 3397–3405.
[49] Galland, C.; Ghosh, Y.; Steinbrück, A.; Sykora, M.; Hollingsworth, J. A.; Klimov, V. I.; Htoon, H. Two types of luminescence blinking revealed by spectroelectrochemistry of single quantum dots. *Nature* **2011**, *479*, 203–207.
[50] Ahmed, T.; Seth, S.; Samanta, A. Mechanistic investigation of the defect activity contributing to the photoluminescence blinking of $CsPbBr_3$ perovskite nanocrystals. *ACS Nano* **2019**, *13*, 13537–13544.
[51] Osad'ko, I. S. Two types of the relation between the intensity and the life time of photoluminescence of core/shell semiconductor quantum dots: Important role of coulomb field and tunneling transitions. *J. Chem. Phys.* **2014**, *141*, 164312.
[52] Trinh, C. T.; Minh, D. N.; Ahn, K. J.; Kang, Y.; Lee, K. G. Verification of type-A and type-B-HC blinking mechanisms of organic–inorganic formamidinium lead halide perovskite quantum dots by FLID measurements. *Sci. Rep.* **2020**, *10*, 2172.
[53] Hu, F. R.; Yin, C. Y.; Zhang, H. C.; Sun, C.; Yu, W. W.; Zhang, C. F.; Wang, X. Y.; Zhang, Y.; Xiao, M. Slow Auger recombination of charged excitons in nonblinking perovskite nanocrystals without spectral diffusion. *Nano Lett.* **2016**, *16*, 6425–6430.
[54] Ihara, T.; Kanemitsu, Y. Spectral diffusion of neutral and charged exciton transitions in single CdSe/ZnS nanocrystals due to quantum-confined stark effect. *Phys. Rev. B* **2014**, *90*, 195302.
[55] Han, X.; Zhang, G. F.; Li, B.; Yang, C. G.; Guo, W. L.; Bai, X. Q.; Huang, P.; Chen, R. Y.; Qin, C. B.; Hu, J. Y. et al. Blinking mechanisms and intrinsic quantum-confined stark effect in single methylammonium lead bromide perovskite quantum dots. *Small* **2020**, *16*, 2005435.
[56] Zhang, G. F.; Peng, Y. G.; Xie, H. Q.; Li, B.; Li, Z. J.; Yang, C. G.; Guo, W. L.; Qin, C. B.; Chen, R. Y.; Gao, Y. et al. Linear dipole behavior of single quantum dots encased in metal oxide semiconductor nanoparticles films. *Front. Phys.* **2019**, *14*, 23605.
[57] Hiroshige, N.; Ihara, T.; Kanemitsu, Y. Simultaneously measured photoluminescence lifetime and quantum yield of two-photon cascade emission on single CdSe/ZnS nanocrystals. *Phys. Rev. B* **2017**, *95*, 245307.
[58] Vaxenburg, R.; Rodina, A.; Lifshitz, E.; Efros, A. L. Biexciton Auger recombination in CdSe/CdS core/shell semiconductor nanocrystals. *Nano Lett.* **2016**, *16*, 2503–2511.
[59] Lin, W. Z.; Niu, Y.; Meng, R. Y.; Huang, L.; Cao, H. J.; Zhang, Z. X.; Qin, H. Y.; Peng, X. G. Shell-thickness dependent optical properties of CdSe/CdS core/shell nanocrystals coated with thiol ligands. *Nano Res.* **2016**, *9*, 260–271.
[60] Yuan, G. C.; Ritchie, C.; Ritter, M.; Murphy, S.; Gómez, D. E.; Mulvaney, P. The degradation and blinking of single $CsPbI_3$ perovskite quantum dots. *J. Phys. Chem. C* **2018**, *122*, 13407–13415.
[61] Li, B.; Huang, H.; Zhang, G. F.; Yang, C. G.; Guo, W. L.; Chen, R. Y.; Qin, C. B.; Gao, Y.; Biju, V. P.; Rogach, A. L. et al. Excitons and biexciton dynamics in single $CsPbBr_3$ perovskite quantum dots. *J. Phys. Chem. Lett.* **2018**, *9*, 6934–6940.
[62] Yang, C. G.; Li, Y.; Hou, X. Q.; Zhang, M.; Zhang, G. F.; Li, B.; Guo, W. L.; Han, X.; Bai, X. Q.; Li, J. L. et al. Conversion of photoluminescence blinking types in single colloidal quantum dots. *Small*, in press, https://doi.org/10.1002/smll.202309134.
[63] Morozov, S.; Pensa, E. L.; Khan, A. H.; Polovitsyn, A.; Cortés, E.; Maier, S. A.; Vezzoli, S.; Moreels, I.; Sapienza, R. Electrical control of single-photon emission in highly charged individual colloidal quantum dots. *Sci. Adv.* **2020**, *6*, eabb1821.
[64] LeBlanc, S. J.; McClanahan, M. R.; Moyer, T.; Jones, M.; Moyer, P. J. Fluorescence modulation in single CdSe quantum dots by moderate applied electric fields. *J. Appl. Phys.* **2014**, *115*, 034306.
[65] Trinh, C. T.; Minh, D. N.; Nguyen, V. L.; Ahn, K. J.; Kang, Y.; Lee, K. G. An experimental study on the blinking suppression mechanism of organic-inorganic formamidinium lead halide perovskite quantum dots on N-type semiconductors. *APL Mater.* **2020**, *8*, 031102.
[66] Li, B.; Zhang, G. F.; Wang, Z.; Li, Z. J.; Chen, R. Y.; Qin, C. B.; Gao, Y.; Xiao, L. T.; Jia, S. T. Suppressing the fluorescence blinking of single quantum dots encased in N-type semiconductor nanoparticles. *Sci. Rep.* **2016**, *6*, 32662.
[67] Sayevich, V.; Robinson, Z. L.; Kim, Y.; Kozlov, O. V.; Jung, H.; Nakotte, T.; Park, Y. S.; Klimov, V. I. Highly versatile near-infrared emitters based on an atomically defined HgS interlayer embedded into a CdSe/CdS quantum dot. *Nat. Nanotechnol.* **2021**, *16*, 673–679.
[68] Krishnamurthy, S.; Singh, A.; Hu, Z. J.; Blake, A. V.; Kim, Y.; Singh, A.; Dolgopolova, E. A.; Williams, D. J.; Piryatinski, A.; Malko, A. V. et al. PbS/CdS quantum dot room-temperature single-emitter spectroscopy reaches the telecom O and s bands via an engineered stability. *ACS Nano* **2021**, *15*, 575–587.
[69] Chen, O.; Zhao, J.; Chauhan, V. P.; Cui, J.; Wong, C.; Harris, D. K.; Wei, H.; Han, H. S.; Fukumura, D.; Jain, R. K. et al. Compact high-quality CdSe-CdS core–shell nanocrystals with narrow emission linewidths and suppressed blinking. *Nat. Mater.* **2013**, *12*, 445–451.
[70] Jain, A.; Voznyy, O.; Hoogland, S.; Korkusinski, M.; Hawrylak, P.; Sargent, E. H. Atomistic design of CdSe/CdS core–shell quantum dots with suppressed Auger recombination. *Nano Lett.* **2016**, *16*, 6491–6496.
[71] Hou, X. Q.; Li, Y.; Qin, H. Y.; Peng, X. G. Effects of interface-potential smoothness and wavefunction delocalization on Auger

recombination in colloidal CdSe-based core/shell quantum dots. *J. Chem. Phys.* **2019**, *151*, 234703.
[72] Guo, W. L.; Tang, J. L.; Zhang, G. F.; Li, B.; Yang, C. G.; Chen, R. Y.; Qin, C. B.; Hu, J. Y.; Zhong, H. Z.; Xiao, L. T. et al. Photoluminescence blinking and biexciton Auger recombination in single colloidal quantum dots with sharp and smooth core/shell interfaces. *J. Phys. Chem. Lett.* **2021**, *12*, 405–412.
[73] Hu, Z.; Liu, S. J.; Qin, H. Y.; Zhou, J. H.; Peng, X. G. Oxygen stabilizes photoluminescence of CdSe/CdS core/shell quantum dots via deionization. *J. Am. Chem. Soc.* **2020**, *142*, 4254–4264.
[74] Yang, C. G.; Zhang, G. F.; Feng, L. H.; Li, B.; Li, Z. J.; Chen, R. Y.; Qin, C. B.; Gao, Y.; Xiao, L. T.; Jia, S. T. Suppressing the photobleaching and photoluminescence intermittency of single near-infrared CdSeTe/ZnS quantum dots with p-Phenylenediamine. *Opt. Express* **2018**, *26*, 11889–11902.
[75] Thomas, E. M.; Ghimire, S.; Kohara, R.; Anil, A. N.; Yuyama, K. I.; Takano, Y.; Thomas, K. G.; Biju, V. Blinking suppression in highly excited CdSe/ZnS quantum dots by electron transfer under large positive Gibbs (free) energy change. *ACS Nano* **2018**, *12*, 9060–9069.
[76] Chouhan, L.; Ito, S.; Thomas, E. M.; Takano, Y.; Ghimire, S.; Miyasaka, H.; Biju, V. Real-time blinking suppression of perovskite quantum dots by halide vacancy filling. *ACS Nano* **2021**, *15*, 2831–2838.
[77] Huang, X. N.; Xu, Q. F.; Zhang, C. F.; Wang, X. Y.; Xiao, M. Energy transfer of biexcitons in a single semiconductor nanocrystal. *Nano Lett.* **2016**, *16*, 2492–2496.
[78] Nair, G.; Zhao, J.; Bawendi, M. G. Biexciton quantum yield of single semiconductor nanocrystals from photon statistics. *Nano Lett.* **2011**, *11*, 1136–1140.
[79] Paulite, M.; Acharya, K. P.; Nguyen, H. M.; Hollingsworth, J. A.; Htoon, H. Inverting asymmetric confinement potentials in core/thick-shell nanocrystals. *J. Phys. Chem. Lett.* **2015**, *6*, 706–711.
[80] Xu, W. W.; Hou, X. Q.; Meng, Y. J.; Meng, R. Y.; Wang, Z. Y.; Qin, H. Y.; Peng, X. G.; Chen, X. W. Deciphering charging status, absolute quantum efficiency, and absorption cross section of multicarrier states in single colloidal quantum dots. *Nano Lett.* **2017**, *17*, 7487–7493.
[81] Li, B.; Zhang, G. F.; Zhang, Y.; Yang, C. G.; Guo, W. L.; Peng, Y. G.; Chen, R. Y.; Qin, C. B.; Gao, Y.; Hu, J. Y. et al. Biexciton dynamics in single colloidal CdSe quantum dots. *J. Phys. Chem. Lett.* **2020**, *11*, 10425–10432.
[82] Cihan, A. F.; Martinez, P. L. H.; Kelestemur, Y.; Mutlugun, E.; Demir, H. V. Observation of biexcitons in nanocrystal solids in the presence of photocharging. *ACS Nano* **2013**, *7*, 4799–4809.
[83] Vonk, S. J. W.; Heemskerk, B. A. J.; Keitel, R. C.; Hinterding, S. O. M.; Geuchies, J. J.; Houtepen, A. J.; Rabouw, F. T. Biexciton binding energy and line width of single quantum dots at room temperature. *Nano Lett.* **2021**, *21*, 5760–5766.
[84] Lubin, G.; Tenne, R.; Ulku, A. C.; Antolovic, I. M.; Burri, S.; Karg, S.; Yallapragada, V. J.; Bruschini, C.; Charbon, E.; Oron, D. Heralded spectroscopy reveals exciton–exciton correlations in single colloidal quantum dots. *Nano Lett.* **2021**, *21*, 6756–6763.
[85] Li, Z. J.; Zhang, G. F.; Li, B.; Chen, R. Y.; Qin, C. B.; Gao, Y.; Xiao, L. T.; Jia, S. T. Enhanced biexciton emission from single quantum dots encased in N-type semiconductor nanoparticles. *Appl. Phys. Lett.* **2017**, *111*, 153106.
[86] Krivenkov, V.; Goncharov, S.; Samokhvalov, P.; Sánchez-Iglesias, A.; Grzelczak, M.; Nabiev, I.; Rakovich, Y. Enhancement of biexciton emission due to long-range interaction of single quantum dots and gold nanorods in a thin-film hybrid nanostructure. *J. Phys. Chem. Lett.* **2019**, *10*, 481–486.
[87] Masuo, S.; Kanetaka, K.; Sato, R.; Teranishi, T. Direct observation of multiphoton emission enhancement from a single quantum dot using AFM manipulation of a cubic gold nanoparticle. *ACS Photonics* **2016**, *3*, 109–116.
[88] Naiki, H.; Oikawa, H.; Masuo, S. Modification of emission photon statistics from single quantum dots using metal/SiO_2 core/shell nanostructures. *Photochem. Photobiol. Sci.* **2017**, *16*, 489–498.
[89] Hiroshige, N.; Ihara, T.; Saruyama, M.; Teranishi, T.; Kanemitsu, Y. Coulomb-enhanced radiative recombination of biexcitons in single giant-shell CdSe/CdS core/shell nanocrystals. *J. Phys. Chem. Lett.* **2017**, *8*, 1961–1966.
[90] Rabouw, F. T.; Vaxenburg, R.; Bakulin, A. A.; van Dijk-Moes, R. J. A.; Bakker, H. J.; Rodina, A.; Lifshitz, E.; Efros, A. L.; Koenderink, A. F.; Vanmaekelbergh, D. Dynamics of intraband and interband Auger processes in colloidal core–shell quantum dots. *ACS Nano* **2015**, *9*, 10366–10376.
[91] Ma, X. D.; Diroll, B. T.; Cho, W.; Fedin, I.; Schaller, R. D.; Talapin, D. V.; Gray, S. K.; Wiederrecht, G. P.; Gosztola, D. J. Size-dependent biexciton quantum yields and carrier dynamics of quasi-two-dimensional core/shell nanoplatelets. *ACS Nano* **2017**, *11*, 9119–9127.
[92] Mangum, B. D.; Sampat, S.; Ghosh, Y.; Hollingsworth, J. A.; Htoon, H.; Malko, A. V. Influence of the core size on biexciton quantum yield of giant CdSe/CdS nanocrystals. *Nanoscale* **2014**, *6*, 3712–3720.
[93] Park, Y. S.; Bae, W. K.; Padilha, L. A.; Pietryga, J. M.; Klimov, V. I. Effect of the core/shell interface on Auger recombination evaluated by single-quantum-dot spectroscopy. *Nano Lett.* **2014**, *14*, 396–402.
[94] Mangum, B. D.; Ghosh, Y.; Hollingsworth, J. A.; Htoon, H. Disentangling the effects of clustering and multi-exciton emission in second-order photon correlation experiments. *Opt. Express* **2013**, *21*, 7419–7426.
[95] Mishra, N.; Orfield, N. J.; Wang, F.; Hu, Z. J.; Krishnamurthy, S.; Malko, A. V.; Casson, J. L.; Htoon, H.; Sykora, M.; Hollingsworth, J. A. Using shape to turn off blinking for two-colour multiexciton emission in CdSe/CdS tetrapods. *Nat. Commun.* **2017**, *8*, 15083.
[96] Eloi, F.; Frederich, H.; Leray, A.; Buil, S.; Quélin, X.; Ji, B.; Giovanelli, E.; Lequeux, N.; Dubertret, B.; Hermier, J. P. Unraveling the time cross correlations of an emitter switching between two states with the same fluorescence intensity. *Opt. Express* **2015**, *23*, 29921–29928.
[97] Feng, S. W.; Cheng, C. Y.; Wei, C. Y.; Yang, J. H.; Chen, Y. R.; Chuang, Y. W.; Fan, Y. H.; Chuu, C. S. Purification of single photons from room-temperature quantum dots. *Phys. Rev. Lett.* **2017**, *119*, 143601.
[98] Ta, H.; Keller, J.; Haltmeier, M.; Saka, S. K.; Schmied, J.; Opazo, F.; Tinnefeld, P.; Munk, A.; Hell, S. W. Mapping molecules in scanning far-field fluorescence nanoscopy. *Nat. Commun.* **2015**, *6*, 7977.
[99] Li, B.; Zhang, G. F.; Yang, C. G.; Li, Z. J.; Chen, R. Y.; Qin, C. B.; Gao, Y.; Huang, H.; Xiao, L. T.; Jia, S. T. Fast recognition of single quantum dots from high multi-exciton emission and clustering effects. *Opt. Express* **2018**, *26*, 4674–4685.
[100] Li, B.; Gao, Y. K.; Wu, R. X.; Miao, X. Y.; Zhang, G. F. Charge and energy transfer dynamics in single colloidal quantum dots/monolayer MoS_2 heterostructures. *Phys. Chem. Chem. Phys.* **2023**, *25*, 8161–8167.
[101] Zhai, X. T.; Zhang, R. X.; Sheng, H. X.; Wang, J.; Zhu, Y. M.; Lu, Z. C.; Li, Z. Y.; Huang, X.; Li, H.; Lu, G. Direct observation of the light-induced exfoliation of molybdenum disulfide sheets in water medium. *ACS Nano* **2021**, *15*, 5661–5670.
[102] Chen, Y. Q.; Li, Z. Y.; Huang, X.; Lu, G.; Huang, W. Single-molecule mapping of catalytic reactions on heterostructures. *Nano Today* **2020**, *34*, 100957.
[103] Li, Z. Y.; Devasenathipathy, R.; Wang, J. J.; Yu, L. Y. Z.; Liang, Y.; Sheng, H. X.; Zhu, Y. M.; Li, H.; Uji-i, H.; Huang, X. et al. Direct observation of the plasmon-enhanced palladium catalysis with single-molecule fluorescence microscopy. *Nano Res.* **2023**, *16*, 8817–8826.
[104] Houel, J.; Doan, Q. T.; Cajgfinger, T.; Ledoux, G.; Amans, D.; Aubret, A.; Dominjon, A.; Ferriol, S.; Barbier, R.; Nasilowski, M. et al. Autocorrelation analysis for the unbiased determination of power-law exponents in single-quantum-dot blinking. *ACS Nano* **2015**, *9*, 886–893.
[105] Zhang, G. F.; Rocha, S.; Lu, G.; Yuan, H. F.; Uji-i, H.; Floudas, G. A.; Müllen, K.; Xiao, L. T.; Hofkens, J.; Debroye, E. Spatially and temporally resolved heterogeneities in a miscible polymer blend. *ACS Omega* **2020**, *5*, 23931–23939.

[106] Zhang, G. F.; Li, B.; Chen, R. Y.; Qin, C. B.; Gao, Y.; Xiao, L. T.; Jia, S. T. Single-molecule probes revealed dynamics of confined nano-regions in miscible polymer blends. *Acta Phys. Sin.* **2019**, *68*, 148201.

[107] Tachikawa, T.; Karimata, I.; Kobori, Y. Surface charge trapping in organolead halide perovskites explored by single-particle photoluminescence imaging. *J. Phys. Chem. Lett.* **2015**, *6*, 3195–3201.

[108] Tian, W. M.; Zhao, C. Y.; Leng, J.; Cui, R. R.; Jin, S. Y. Visualizing carrier diffusion in individual single-crystal organolead halide perovskite nanowires and nanoplates. *J. Am. Chem. Soc.* **2015**, *137*, 12458–12461.

[109] Hensgens, T.; Fujita, T.; Janssen, L.; Li, X.; Van Diepen, C. J.; Reichl, C.; Wegscheider, W.; Das Sarma, S.; Vandersypen, L. M. K. Quantum simulation of a Fermi–Hubbard model using a semiconductor quantum dot array. *Nature* **2017**, *548*, 70–73.

[110] Tang, J. S.; Zhou, Z. Q.; Wang, Y. T.; Li, Y. L.; Liu, X.; Hua, Y. L.; Zou, Y.; Wang, S.; He, D. Y.; Chen, G. et al. Storage of multiple single-photon pulses emitted from a quantum dot in a solid-state quantum memory. *Nat. Commun.* **2015**, *6*, 8652.

[111] Proppe, A. H.; Berkinsky, D. B.; Zhu, H.; Šverko, T.; Kaplan, A. E. K.; Horowitz, J. R.; Kim, T.; Chung, H.; Jun, S.; Bawendi, M. G. Highly stable and pure single-photon emission with 250 ps optical coherence times in InP colloidal quantum dots. *Nat. Nanotechnol.* **2023**, *18*, 993–999.

[112] Berkinsky, D. B.; Proppe, A. H.; Utzat, H.; Krajewska, C. J.; Sun, W. W.; Šverko, T.; Yoo, J. J.; Chung, H.; Won, Y. H.; Kim, T. et al. Narrow intrinsic line widths and electron–phonon coupling of InP colloidal quantum dots. *ACS Nano* **2023**, *17*, 3598–3609.

[113] Utzat, H.; Sun, W. W.; Kaplan, A. E. K.; Krieg, F.; Ginterseder, M.; Spokoyny, B.; Klein, N. D.; Shulenberger, K. E.; Perkinson, C. F.; Kovalenko, M. V. et al. Coherent single-photon emission from colloidal lead halide perovskite quantum dots. *Science* **2019**, *363*, 1068–1072.

[114] Liu, J. Q.; Zhu, C.; Pols, M.; Zhang, Z.; Hu, F. R.; Wang, L.; Zhang, C. F.; Liu, Z.; Tao, S. X.; Xiao, M. et al. Discrete elemental distributions inside a single mixed-halide perovskite nanocrystal for the self-assembly of multiple quantum-light sources. *Nano Lett.* **2023**, *23*, 10089–10096.